

Journal of Astronomical Telescopes, Instruments, and Systems

AstronomicalTelescopes.SPIEDigitalLibrary.org

Fast optimal design of a flexure for lightweight, horizontally supported mirror

Pingwei Zhou
Shuyan Xu
Changxiang Yan
Xiaohui Zhang

SPIE.

Pingwei Zhou, Shuyan Xu, Changxiang Yan, Xiaohui Zhang, "Fast optimal design of a flexure for lightweight, horizontally supported mirror," *J. Astron. Telesc. Instrum. Syst.* **5**(2), 024001 (2019), doi: 10.1117/1.JATIS.5.2.024001.

Fast optimal design of a flexure for lightweight, horizontally supported mirror

Pingwei Zhou,^{a,b,*} Shuyan Xu,^a Changxiang Yan,^a and Xiaohui Zhang^a

^aChinese Academy of Sciences, Changchun Institute of Optics, Fine Mechanics and Physics, Changchun, China

^bUniversity of Chinese Academy of Sciences, Beijing, China

Abstract. Due to optical performance requirements, the primary mirror assembly must have the ability to be unaffected by environmental influences. These environmental influences include gravity, assembly error, and thermal change, by which external loads are imposed on the mirror. The external loads degrade the mirror surface accuracy and cause misalignment between mirrors. We describe a method to determine the allowable external loads. The performance of a flexure is evaluated by the transmitted loads to the mirror. The force acting on the mirror was analyzed under various conditions and the influence functions were obtained using inertia relief. With the knowledge of influence functions, the relationship between external loads and mirror surface distortion was built. According to the error budget of the primary mirror, the permissible loads required of the flexure were directly established. The optimization was achieved through optimizing the compliance of the flexure without mirror. With our method, the mirror design and flexure design are decoupled, and time and resources required for optimization are reduced. A parallel flexure is demonstrated for a 2-m lightweight, horizontally supported mirror. © 2019 Society of Photo-Optical Instrumentation Engineers (SPIE) [DOI: 10.1117/1.JATIS.5.2.024001]

Keywords: flexure design; optimization; external loads; surface distortion.

Paper 18114 received Nov. 19, 2018; accepted for publication Apr. 1, 2019; published online Apr. 16, 2019.

1 Introduction

Astronomical and Earth observations performed using space telescopes have become increasingly popular in recent years. Space observation has many advantages, including avoidance of the effects of weather and image fluctuations due to atmospheric flow. It also enables multispectral detection, which offers more information than Earth-based observations.¹ However, space telescopes must be weight-constrained and able to resist environmental influences, such as gravity, assembly error, thermal change, and launch.² The primary mirror is the heaviest component in the telescope so it needs to be lightweight designed. However, the lightweighting reduces the rigidity of the primary mirror, and surface distortion under gravity thereby increases. Manufacturing tolerances on parallelism between the mounting interfaces on the baseplate impose the requirement that each support accommodate a fixed angular displacement in any orientation during assembly. The resulting moment on the mirror must not cause excessive mirror surface distortion. Due to the differences in coefficients of the thermal expansion, the thermal changes during ground test and in the space environment cause a differential thermal expansion or contraction between primary mirror and the baseplate. For the optical performance to remain unaffected by the environmental influences, a flexure must be compliant to absorb the external loads, passively.³ The launch environment, on the other hand, imposes the requirement on the flexure that the maximum stress during launch must not exceed the microyield of the material.⁴ The flexure satisfying that requirement is also necessarily stiff, which can be estimated by the fundamental frequency.

In the traditional optimization procedure, the supporting performance of a flexure has to be evaluated by analyzing the mirror assembly finite element analysis (FEA) model including flexures. For the large aperture primary mirror, the analysis time is long. Furthermore, exhaustive iterations with modeling and FEA are required to satisfy different requirements simultaneously.⁵ Due to the two reasons mentioned above, the optimal design is time consuming. In this study, we demonstrate a method to determine the allowable external loads that cause the degradation of lightweight mirror surface accuracy and misalignment between mirrors. First, the force and deformation analysis at the free end of flexure under gravity, assembly error, and thermal change were performed. Second, the relationship between the transmitted loads and the mirror surface distortion was built based on the influence functions obtained from inertia relief analysis. This relationship was verified by comparing the result of superposing influence functions scaled by according transmitted load and with that of primary mirror assembly FEA model. At last, according to the error budget and the influence functions, the permissible loads required of the flexure were directly established. The optimization was achieved through optimizing the compliance of the flexure under three simple load cases. The results after optimization were within the error budget simultaneously.

2 Mirror and Support Configuration

In this study, a partially closed back monolithic, SiC primary mirror configuration is examined. Some advantages of the partially closed back design include higher mirror flexural rigidity relative to open-back designs and fabrication simplicity relative to built-up configurations. The aperture is 2.0 m, the radius of

*Address all correspondence to Pingwei Zhou, E-mail: npuzhoupw@163.com

curvature is 10.5 m, the supporting radius is 0.68 m, the depth is 0.18 m, and the mass is 265 kg. The length of the side of triangular isogrid is 0.139 m and the intersections have 0.08 m inscribed circle diameter. To improve the thermal stability, three invar sleeves, which have the same expansion coefficient with SiC material, are bonded to the internal surface of supporting holes using epoxy adhesive [GHJ-01(Z)] in a 120-deg interval. And the thickness of applied epoxy is 10 μm , which is controlled by hollow microspheres. The 10- μm microspheres are first mixed evenly with adhesive evenly at a mass fraction of 3%. Then, the mixture is applied at the bonding area. The primary mirror is supported by three parallel flexures through the supporting holes located on its back as shown in Fig. 1. The flexure mounting may be regarded as a semikinematic design because it has a finite contact area. The proposed flexure is much the same as a three-prismatic-universal-universal compliant parallel structure⁶ (3PUU), which provides controlled motion through elastic deformation. Three-point support is commonly used in the mirror support of space telescopes due to its simplicity and effectiveness. As the primary mirror subassembly and the telescope are tested and aligned with its optical axis horizontal, the required self-weight distortions can be achieved by three-point supports. Meanwhile, minimizing self-weight distortions on flight mounts without gravity-unloading using counterweights, airbags, or actuators introduces the least uncertainty to test. Compared with biaxial flexure,⁷ parallel flexure has smaller bending stiffness and higher axial stiffness, which allows higher resonant frequency. So each titanium flexure consists of a free end, a fixed end, and three limbs of identical flexural structure. The free end and fixed end of the flexure are attached to sleeves and the baseplate by screws, respectively. The material properties used in the primary mirror assembly are summarized in Table 1.

Due to the requirements of optical performance, the primary mirror assembly must have the ability to be unaffected by

Table 1 Material properties used in the primary mirror assembly.

Material	SiC (mirror)	Invar (sleeve)	Titanium (flexure)	Adhesive
Yong's modulus (Mpa)	330	141	109	0.158
Poisson's ration	0.25	0.25	0.29	0.49
Density (t/mm ³)	3.05×10^{-9}	8.1×10^{-9}	4.4×10^{-9}	1.3×10^{-9}
Coefficient of thermal expansion (1/°C)	2.5×10^{-6}	2.5×10^{-6}	9.1×10^{-6}	3×10^{-3}

environmental influences. These environmental influences include gravity, assembly error, and thermal change, by which external loads are imposed on the mirror. The external loads degrade the mirror surface accuracy and cause misalignment between mirrors. The flexure is used to isolate external loads by passively utilizing its own elastic deformation. So the optical supporting performance of a flexure can be evaluated by the transmitted loads to the mirror. The relationship between the displacements at the free end and the transmitted loads can be formulated as follows:

$$[u_x \ u_y \ u_z \ \theta_x \ \theta_y \ \theta_z]^T = C[F_x \ F_y \ F_z \ M_x \ M_y \ M_z]^T, \tag{1}$$

where F_n and u_n are the force and translational displacement with respect to the n -axis, M_n and θ_n are the moment and rotational displacements about the n -axis, respectively.

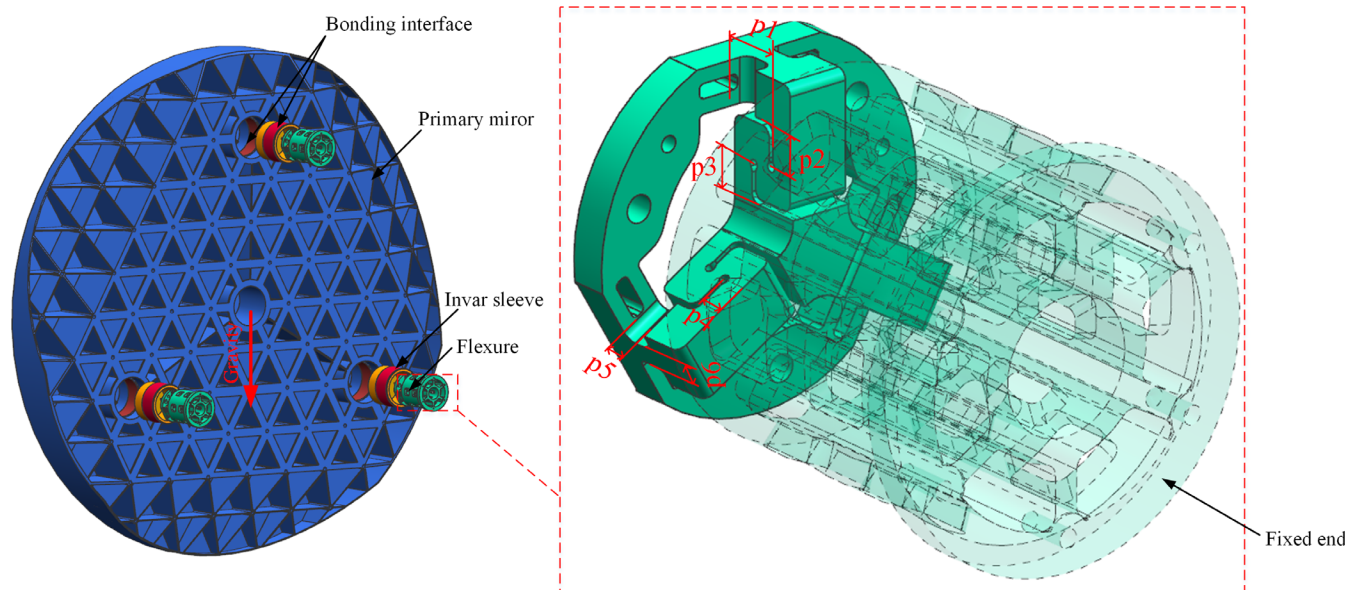


Fig. 1 Exploded view of predesigned lightweight primary mirror assembly showing the symmetries, invar sleeve, and gravity orientation. The indicated parameters of the flexure, which are listed in Table 2, are optimized to satisfy the supporting performance. For clarity, the rigid part of the flexure has been set to transparent.

A few remarks will be made in the following regarding the application of Eq. (1) to the analysis of flexure. First, the flexure mounting is composed of flexible strips and rigid part in which the flexible strips are much more flexible than its connecting parts. That is, the deflection due to shearing is negligible. Second, the flexure strips are assumed to be homogeneous and isotropic. Finally, the compliance matrix C is developed by utilizing Castigliano's displacement theorem, which is formulated based on the strain energy stored through elastic deformations. The compliance matrix C includes 10 independent elements⁸⁻¹⁰ as follows:

$$C = \begin{bmatrix} C_{x-F_x} & 0 & 0 & 0 & 0 & 0 \\ 0 & C_{y-F_y} & 0 & 0 & 0 & C_{y-M_z} \\ 0 & 0 & C_{z-F_z} & 0 & C_{z-M_y} & 0 \\ 0 & 0 & 0 & C_{\theta_x-M_x} & 0 & 0 \\ 0 & 0 & C_{\theta_y-F_z} & 0 & C_{\theta_y-M_y} & 0 \\ 0 & C_{\theta_z-F_y} & 0 & 0 & 0 & C_{\theta_z-M_z} \end{bmatrix}. \quad (2)$$

3 Supporting Performance Analysis

3.1 Gravity

It is convenient to test and align space optical systems when the mirror's optical axis is perpendicular to the gravity direction. Also, ground testing with their optical axes horizontal can result in less distortion than in the vertical orientation.¹¹ The surface distortion under self-weight are related to both the compliance of flexure and the mount position.¹² Figure 2 shows the distribution of the transmitted loads applied for the threefold axisymmetric mirror. When the primary mirror is supported horizontally, the force and deformation equations can be obtained:

$$\begin{cases} F_{x2} = F_{x3} \\ F_{x1} + F_{x2} + F_{x3} = 0 \\ M_{y1} = M_{y2} = M_{y3} \\ \frac{2F_{z1}h}{3} + \frac{F_{z2}h}{3} + \frac{F_{z3}h}{3} + M_{y1} + M_{y2} + M_{y3} = mg\epsilon_1, \\ F_{z1} = F_{z2} = F_{z3} = \frac{mg}{3} \\ u_{z1} = C_{z-F_z}F_{z1} + C_{z-M_y}M_{y1} \\ \theta_{y2} = \theta_{y3} = \theta_{y1} = C_{\theta_y-F_z}F_{z1} + C_{\theta_y-M_y}M_{y1} = 0 \end{cases}, \quad (3)$$

where F_{zi} is the force balancing the gravity, F_{xi} is the axial force, and M_{yi} is the moment about the y axis in which the value of i is 1 to 3. Here, h is the distance from the center of one support hole to the line connecting the centers of the other two support holes, and ϵ_1 is the distance from the free end to the mass center of the primary mirror (CG).

Equation (4) is derived from Eq. (3). It is concluded from Eq. (4) that the value of M_{y1} only depends on the compliance of the flexure and its supported weight. Under the gravity condition, the transmitted loads include the force balancing the gravity, the axial force, and the moment about the y axis, which cause a pure z -axis translation at the free end:

$$\begin{cases} F_{x1} = -2F_{x2} = -2F_{x3} \\ F_{x1}h + 3M_{y1} = mg\epsilon_1 \\ M_{y1} = -\frac{mg}{3} \frac{C_{\theta_y-F_z}}{C_{\theta_y-M_y}} \\ u_{z1} = \frac{C_{z-F_z}C_{\theta_y-M_y} - C_{z-M_y}C_{\theta_y-F_z}}{C_{\theta_y-M_y}} \frac{mg}{3} \end{cases}. \quad (4)$$

Inertia relief is an advanced option in ANSYS that allows you to simulate unconstrained structures in a static analysis. It gets the FEA model to exactly balance the force difference (applied force minus weight) in a static analysis with acceleration body forces over the whole structure so that the reaction on the constraint is zero. During analysis, enough constraints are

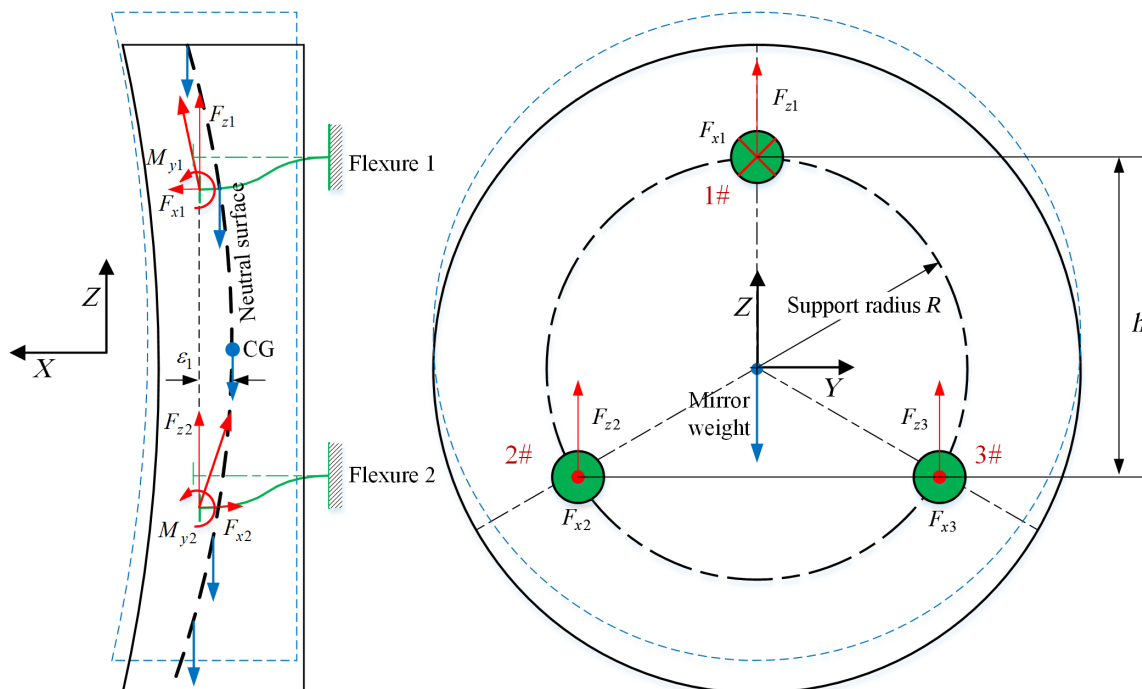


Fig. 2 Schematic distribution of the transmitted loads under self-weight.

required to prevent free body translation and rotation (six for a three-dimensional structure). In this paper, inertia relief is used to analyze the influence functions of external loads. Each influence coefficient represents the effect of one external load on surface distortion. The primary mirror without flexures is to be analyzed as a free-free structure. First, three mass points are established at centers of the three support holes and with different axial location. Second, in order to distribute the external load applied at mass points to the mirror, the RBE3 elements are created to connect the mass points to the nodes on the bonding interface, respectively. The RBE3 element is the flexible connecting element used to distribute loads without introducing additional stiffness of structures. Third, the force balancing the gravity $F_{z1} = F_{z2} = F_{z3} = mg/3$, the unit axial force $F_{x1} = 1\text{ N}$, $F_{x2} = F_{x3} = -0.5\text{ N}$, and the unit moment about the y axis $M_{y1} = M_{y2} = M_{y3} = 1\text{ N} \cdot \text{mm}$ are applied to the mass points. Lastly, three arbitrary nodes apart from the nodes on the bonding interface can be selected as constraint points, in which x degree of freedom is prevented at three nodes, y degree of freedom at two nodes, and z degree of freedom at one node. After each analysis, both force reaction and moment reaction have been calculated to make sure that they are virtually zero. Figure 3 shows the surface distortion in which the

piston and tilt are removed. Figure 3(a) shows the surface distortion δ_G as an example when $F_{z1} = F_{z2} = F_{z3} = mg/3$ is applied at the three mass points with the same axial position of CG. When $F_{z1} = F_{z2} = F_{z3} = mg/3$ is applied at different axial location, the resulting moment causes different surface distortion δ_G accordingly.

In previous research,⁷ the surface distortion δ_A and δ_M , as shown in Figs. 3(b) and 3(c), was used to compensate each of the surface distortion δ_G with different axial position.¹³ The residual surface distortion after compensating and the optimal F_{x1} (17.5 N) remain constant. The residual surface distortion and the result obtained from primary mirror assembly FEA model including flexure when supported at optimum position are shown in Fig. 4. The research indicates that the flexure with different M_{y1} has different optimum mount position ϵ_1 , which can be calculated by bringing $F_{x1} = 17.5\text{ N}$ into Eq. (4). On the contrary, as the mount position ϵ_1 has a range up to 50 mm, the flexure design with a wide range of M_{y1} can be used to support mirror. However, the z -axis translation should be limited to reduce the misalignment between mirrors. As M_{y1} and u_{z1} are either the function of the compliance or parameters of the flexure, a large M_{y1} within the range is preferred.

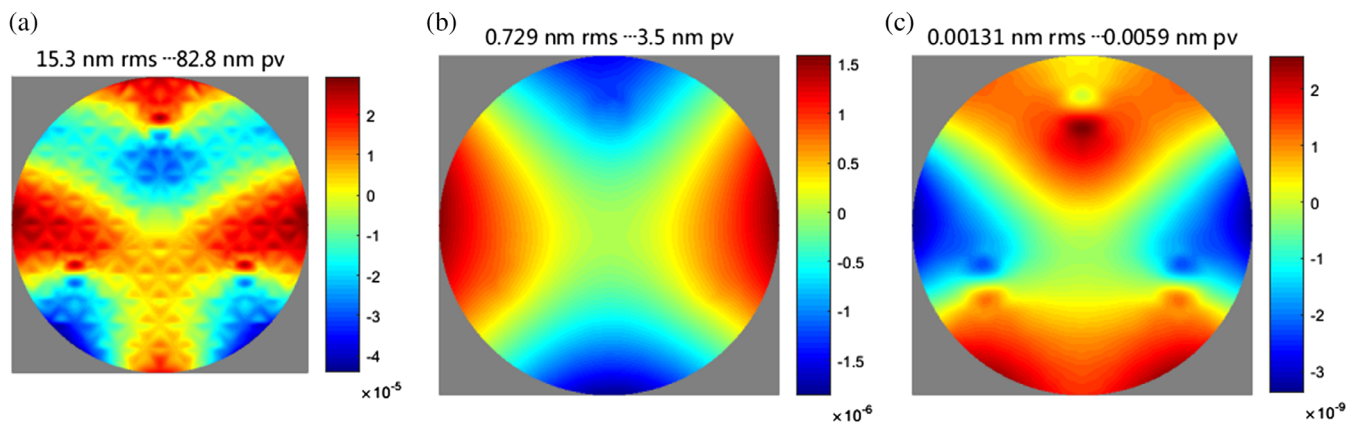


Fig. 3 Influence functions: (a) $F_{z1} = F_{z2} = F_{z3} = \frac{mg}{3}$, (b) $F_{x1} = 1\text{ N}$, $F_{x2} = F_{x3} = -0.5\text{ N}$, and (c) $M_{y1} = M_{y2} = M_{y3} = 1\text{ N} \cdot \text{mm}$.

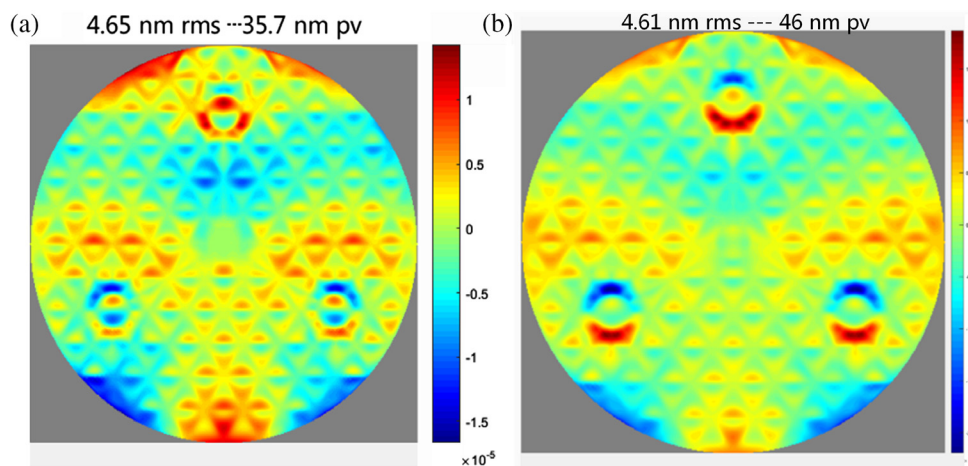


Fig. 4 (a) The residual surface distortion. (b) The surface distortion when supported at optimum mount position.

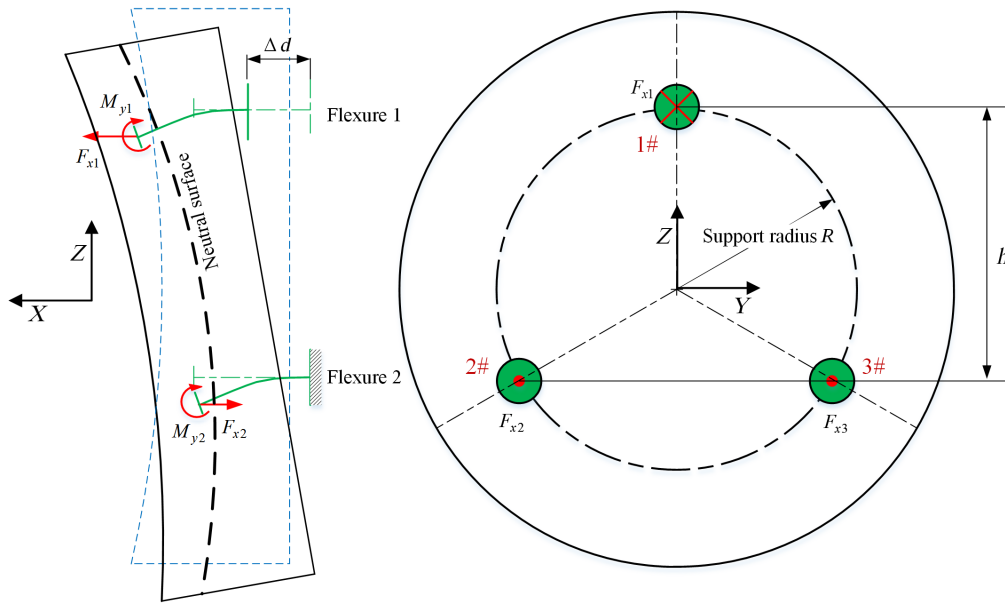


Fig. 5 Schematic distribution of the transmitted loads under assembly error.

3.2 Assembly Error

Manufacturing tolerances on parallelism between the three mounting interfaces on the baseplate impose the requirement that each flexure accommodates a fixed angular displacement in any orientation during assembly. The resulting moment on the mirror must not cause excessive mirror surface distortion. Therefore, the flexure is designed to be bending compliant about orthogonal axes. Figure 5 shows the distribution of the axial force and the resulting moment. Due to the symmetry, the below force and displacement equations can be set up

$$\begin{cases} F_{x2} = F_{x3} \\ F_{x1} + F_{x2} + F_{x3} = 0 \\ F_{z1} = F_{z2} = F_{z3} = 0 \\ M_{y1} = M_{y2} = M_{y3} \\ \frac{2F_{x1}h}{3} + \frac{F_{x2}h}{3} + \frac{F_{x3}h}{3} = M_{y1} + M_{y2} + M_{y3} \\ \theta_{y1} = \theta_{y2} = \theta_{y3} = \text{atan}\left(\frac{\Delta d}{h}\right) \\ \theta_{y1} = C_{\theta_y-F_z} F_{z1} + C_{\theta_y-M_y} M_{y1} \end{cases}, \quad (5)$$

Where Δd is the enforced displacement of one flexure, and the other two flexures keep still.

Under the assembly error, the transmitted loads include the axial force and the moment about the y axis, which cause a pure y-axis rotation. Equation (6) is derived from Eq. (5). It is concluded from Eq. (6) that F_{x1} is related to M_{y1} , the value of M_{y1} only depends on the compliance of the flexure and the y-axis rotation θ_{y1} . Due to the machining accuracy and considering the future deformation of baseplate, Δd is set to 0.1 mm. Then θ_{yi} equals 20.2 in.. The influence functions under assembly error are the same with δ_A and δ_M shown in Figs. 3(b) and 3(c). For a flexure with given value of M_{y1} , the mirror surface distortion under 0.1 mm assembly error can be calculated by $\left(\frac{3\delta_A}{h} + \delta_M\right)M_{y1}$. Figure 6 shows the surface distortion by superposing δ_A and δ_M scaled by the transmitted load and the result under 0.1 mm assembly error, which is obtained from primary mirror assembly FEA model, including the flexure with initial parameters. The unit surface distortion $\frac{3\delta_A}{h} + \delta_M$ is shown in Fig. 7 in which the RMS value represents the RMS influence

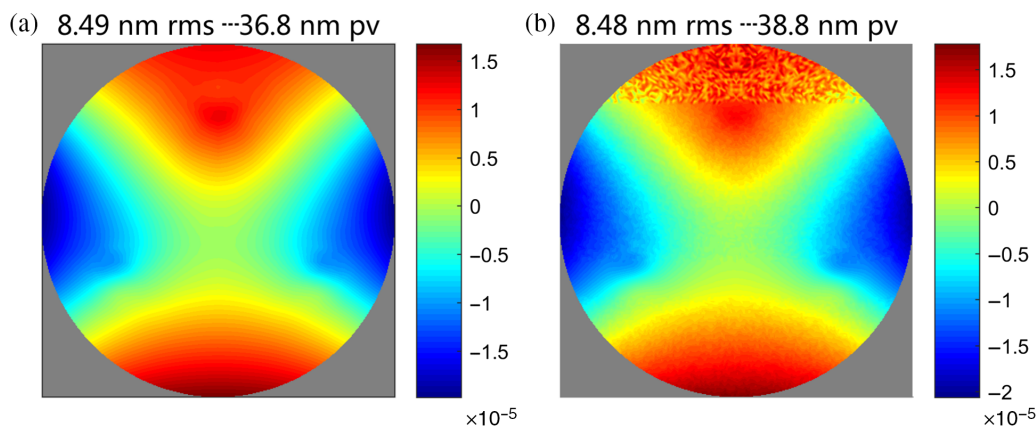


Fig. 6 (a) The superposition result of δ_A and δ_M scaled by the transmitted load. (b) The surface distortion under 0.1 mm assembly error.

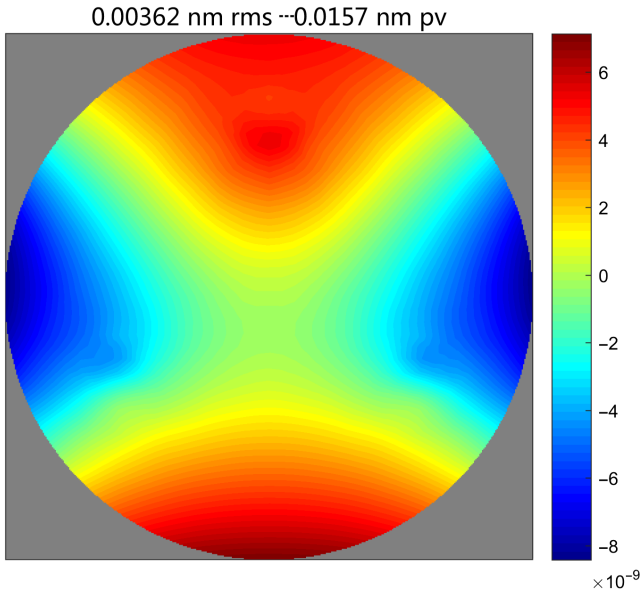


Fig. 7 The unit surface distortion $\frac{\delta_s}{h} + \delta_M$ in which the RMS influence coefficient equals 0.00362 nm.

coefficient. This RMS influence coefficient can be directly scaled to match the allowable RMS value, and the allowable M_{y1} is thereby established:

$$\begin{cases} F_{x1} = -2F_{x2} = -2F_{x3} \\ F_{x1} = \frac{3M_{y1}}{h} \\ M_{y1} = \frac{\theta_{y1}}{C_{\theta_y-M_y}} \end{cases} \quad (6)$$

3.3 Thermal Change

Due to the differences in coefficients of the thermal expansion, the thermal changes during ground test and in the space environment will cause a differential thermal expansion or

contraction between the primary mirror and the baseplate. This differential thermal deformation requires that the flexure is compliant in the radial direction of the axisymmetric mirror. The radial compliance can absorb the differential thermal deformation while maintaining acceptable mirror surface accuracy. Figure 8 shows the distribution of the transmitted loads resulting from temperature raise. Due to the symmetry, the following equations can be obtained:

$$\begin{cases} F_{r1} = F_{r2} = F_{r3} = F_{z1} \\ M_{t1} = M_{t2} = M_{t3} = M_{y1} \\ \theta_t = \theta_{y1} = C_{\theta_y-F_z} F_{z1} + C_{\theta_y-M_y} M_{y1} = 0 \\ u_r = u_{z1} = R\alpha\Delta T = C_{z-F_z} F_{z1} + C_{z-M_y} M_{y1} \end{cases} \quad (7)$$

where F_{ri} and u_r are the force and translational displacement along the radial direction, respectively, and M_{ti} and θ_t are the moment and rotational displacement about the tangential direction, respectively. Here, α is the coefficient of thermal expansion and ΔT is the temperature change.

From Eqs. (1) and (7), we can get

$$\begin{cases} F_{z1} = \frac{C_{\theta_y-M_y}}{C_{z-F_z}C_{\theta_y-M_y} - C_{\theta_y-F_z}C_{z-M_y}} u_{z1} \\ M_{y1} = -\frac{C_{\theta_y-F_z}}{C_{z-F_z}C_{\theta_y-M_y} - C_{\theta_y-F_z}C_{z-M_y}} u_{z1} \\ \beta = \frac{M_{y1}}{F_{z1}} = -\frac{C_{\theta_y-F_z}}{C_{\theta_y-M_y}} \end{cases} \quad (8)$$

Under the thermal change, the transmitted loads include the radial force and the tangential moment cause a pure radial translation. Equation (8) is derived from Eqs. (1) and (7). It is concluded from Eq. (8) that the value of F_{z1} and M_{y1} only depends on the compliance of the flexure and the radial translation u_{z1} . Meanwhile, F_{z1} and M_{y1} are independent of each other and the ratio β is determined by the compliance of the flexure. Due to the operational thermal requirement, ΔT is set to 4°C. Then, u_{z1} equals 6.8 μm . Figure 9 shows the surface distortion δ_R and δ_T in which piston, tilt, and power are removed when $F_{r1} = F_{r2} = F_{r3} = F_{z1} = 1 \text{ N}$ and $M_{t1} = M_{t2} = M_{t3} = M_{y1} = 1 \text{ N} \cdot \text{mm}$ are applied at the three mass points, respectively. It can be

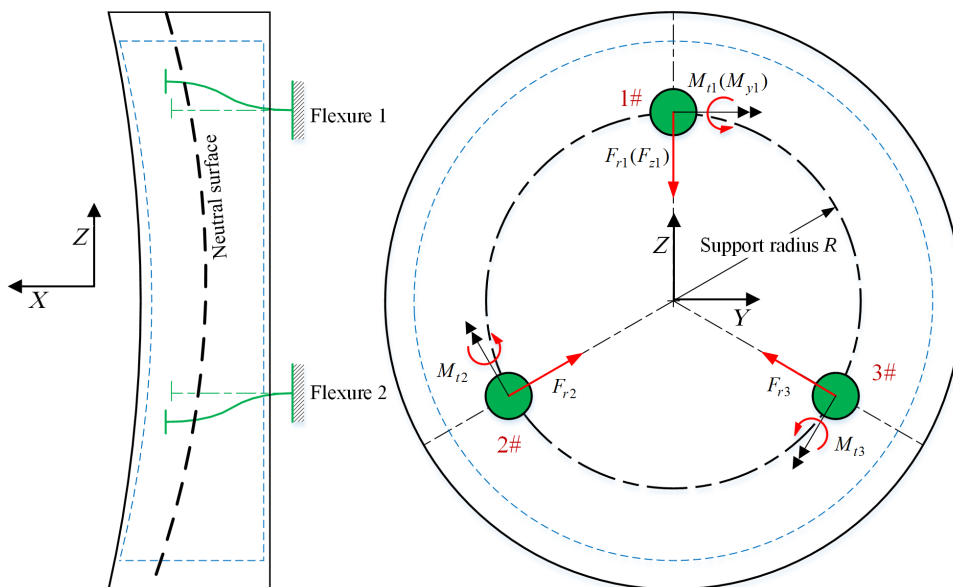


Fig. 8 Schematic distribution of the transmitted loads under thermal change.

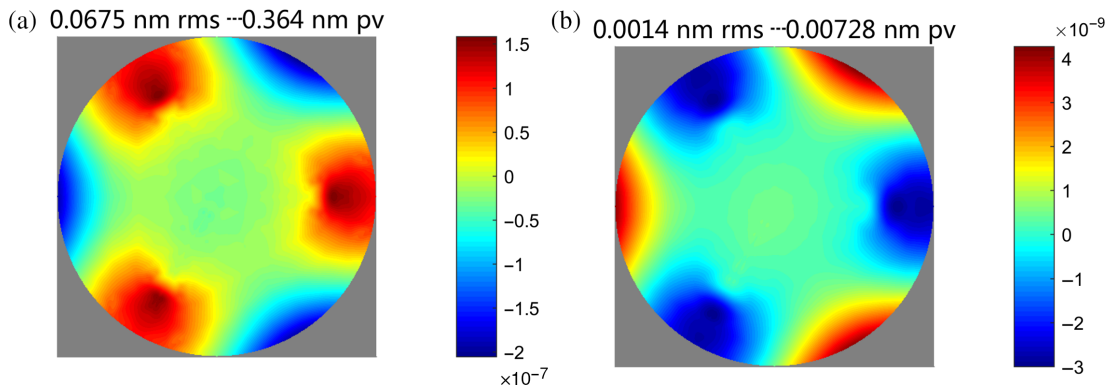


Fig. 9 Influence functions. (a) $F_{r1} = F_{r2} = F_{r3} = 1 \text{ N}$ and (b) $M_{r1} = M_{r2} = M_{r3} = 1 \text{ N} \cdot \text{mm}$.

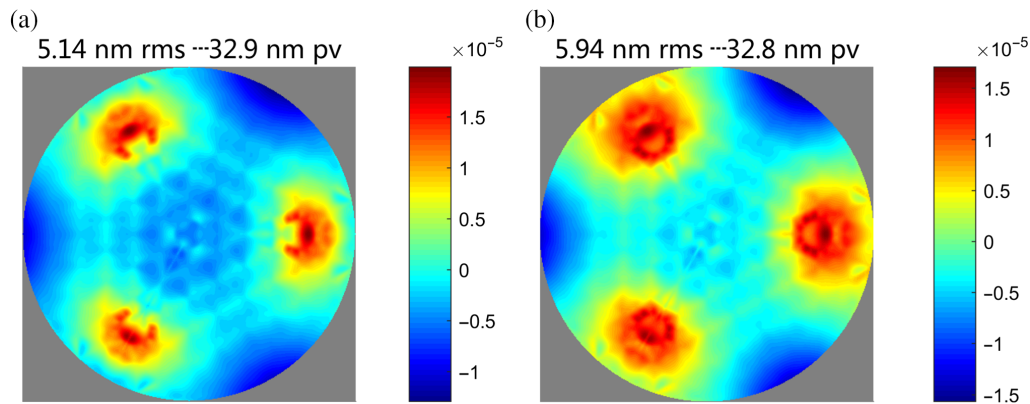


Fig. 10 (a) The superposition result of δ_R and δ_T scaled by the transmitted load. (b) The surface distortion under 4°C thermal change.

seen from Fig. 8 that δ_R and δ_T have the same pattern with the opposite sign. To minimize the surface distortion under thermal change, the ratio β should equal with the RMS value of δ_R divided by that of δ_T . Figure 10 shows the surface distortion by superposing δ_R and δ_T scaled by the transmitted load and the result under 4°C thermal changes, which is obtained from primary mirror assembly FEA model including flexure with initial parameters. The RMS value from superposition is 5.14 nm and 5.94 nm from FEA. The superposition result has not taken the local heat stress into account. This difference can be treated as a system error during optimization.

4 Optimal Design

The influence functions and the error budget of the primary mirror under gravity, 0.1 mm assembly error and 4°C thermal change are summarized in Fig. 11. The error budget defines the allowable RMS surface distortion, the influence functions are scaled to match the error budget, and the allowable transmitted loads are thereby established. Based on the force and deformation analysis in Sec. 3, the transmitted loads to the mirror can be calculated by flexure FEA model without mirror shown in Fig. 11. The analysis time for the primary mirror assembly FEA model including flexures under the three load cases is 15 min, whereas that of flexure FEA model without mirror is 30 s. Given the same iteration number, the resources of the full primary mirror assembly analysis in time are 30 times that of single flexure FEA model. This advantage of less analysis time is more obvious, especially when the closed-form compliance equation for the flexure is developed. The procedure

described above is outlined in the flow diagram shown in Fig. 12. During optimization, the best design of the flexure has the minimum compliance, which reaches the upper limit of the allowable transmitted loads. Because the minimum compliance corresponds to the maximum frequency to resist the launch dynamic loads.² With the proposed procedure, the design task becomes simple and the design period is reduced accordingly.

In this paper, we use UG for parametric modeling, Hypermesh for meshing, Ansys for FEA, and Matlab for superposition of influence functions and rms calculation. The automatic optimization design platform for the flexure is established based on the multidisciplinary optimization software Isight. The multiobjective nondominated sorting genetic algorithm¹⁴ (NSGA-II) is adopted to optimize the flexure to satisfy the targets and constraint listed in Fig. 11. The Dell workstation has 48 CPU cores and 128 GB of memory for parallel-processing. Table 2 summarizes the design parameter, initial values, and optimal values. The initial and optimal performance of the flexure is listed in Table 3. The optimum result obtained from primary mirror assembly is shown in Fig. 13. As shown in Fig. 13, the design error budget is satisfied simultaneously. Considering the different load cases are generally unrelated, the mirror surface accuracy under the combination of the transmitted loads can be calculated by root sum square method (rss).

The design requirement of fundamental frequency is above 100 Hz, which is a great challenge for a three-point supported 2-m mirror assembly. As the flexure is designed to be bending compliant about the orthogonal axes, the first three natural

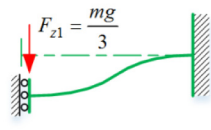
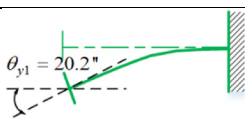
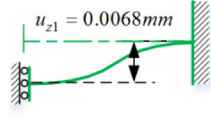
Load cases	Influence coefficients	Allowable RMS	Load and boundary conditions	Target
Self-weight	$\delta_G, \delta_A, \delta_M$	5.5 nm		$u_z \downarrow$ $s.t. M_{y1} = \langle 0 \sim 45000 \text{ N}\cdot\text{mm} \rangle$
0.1 mm assembly error	δ_A, δ_M	4 nm		$\downarrow M_{y1} \leq \frac{4}{0.00362} = 1105 \text{ N}\cdot\text{mm}$
4 °C tempertue change	δ_R, δ_T	5 nm		$\beta = \frac{M_{y1}}{F_{z1}} \Rightarrow \frac{\text{RMS}_{\delta_R}}{\text{RMS}_{\delta_T}} = 48.2$

Fig. 11 Summary of the influence functions and the error budget.

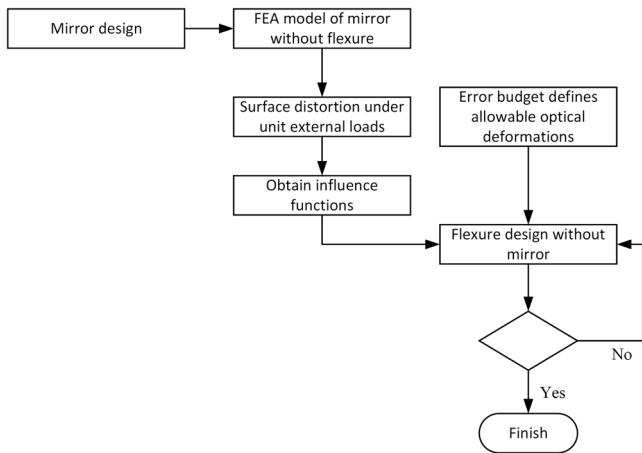


Fig. 12 Flow diagram for fast optimal design of flexure.

Table 2 Summary of design parameter, initial values, variation range, and optimal values.

Parameter	Initial value (mm)	Variation range (mm)	Optimal value (mm)
p1	21	18 to 25	20
p2	15	10 to 18	12.5
p3	15	10 to 18	12.5
p4	9	6 to 12	8
p5	12	10 to 15	13.5
p6	9	6 to 12	7

modes of flexure itself are rotation about the orthogonal axes. The value of the fundamental frequency is 404.3 Hz. However, when calculating the modes of mirror assembly with three flexures, the fundamental frequency is depending on the axial stiffness of flexures. The first mode of mirror assembly is tilt. The mode or frequency of the flexure is not directly related to that of mirror assembly. After optimization, the fundamental frequency of the 2-m mirror assembly has been improved from 79 to 108 Hz. An aluminum dummy mirror, which has the same mass and rigidity with SiC mirror shown in Fig. 1, has been fabricated. As the flexure is still in the process of machining, the vibration test will be performed in near future to verify the computational results using FEA and influence under launch loads. As the processing cycle of the 2-m primary mirror is almost 2 years, the optical supporting performance of a flexure can hardly be verified in advance. However, with the method presented in this paper, the optical supporting performance can be estimated by testing the specific compliance of the

Table 3 Summary of initial and optimal performance by superposition of influence functions.

Load cases	Initial	Optimal
Gravity	$M_{y1} = 38097.9 \text{ N}\cdot\text{mm}$ RMS = 4.65 nm $u_{z1} = 14.1 \mu\text{m}$	$M_{y1} = 41123.7 \text{ N}\cdot\text{mm}$ RMS = 4.65 nm $u_{z1} = 12.6 \mu\text{m}$
0.1 mm assembly error	$M_{y1} = 2347.2 \text{ N}\cdot\text{mm}$ RMS = 8.49 nm	$M_{y1} = 1028.5 \text{ N}\cdot\text{mm}$ RMS = 3.43 nm
4 temperature change	$F_{z1} = 445.3 \text{ N}$, $M_{y1} = 18360.6 \text{ N}\cdot\text{mm}$ $\alpha = \frac{M_{y1}}{F_{z1}} = 41.2$ RMS = 5.14 nm	$F_{z1} = 498.8 \text{ N}$, $M_{y1} = 22185.4 \text{ N}\cdot\text{mm}$ $\beta = \frac{M_{y1}}{F_{z1}} = 44.5$ RMS = 3.4 nm
Frequency	79 Hz	108 Hz

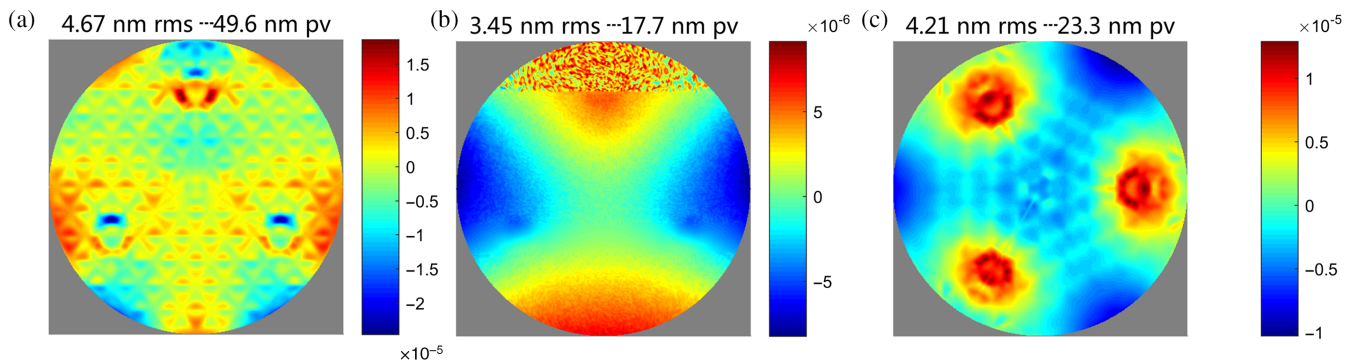


Fig. 13 The optimum result under the three load cases: (a) gravity, (b) 0.1 mm assembly error, and (c) 4 thermal change.

flexure. Then, the static and dynamic requirement of the flexure can be verified in advance.

5 Conclusion

This paper presents a method to determine the allowable external loads that cause the degradation of lightweight mirror surface accuracy and misalignment between mirrors. The force and deformation analyses at the free end of flexure under gravity, assembly error, and thermal change were performed. Based on the above analyses, the force status and characteristic of deformation were summarized in detail. Under gravity, the free end of flexure has a pure z translation and takes a third of gravity. Under 0.1 mm assembly error, the free end of flexure has a pure 20.2 in y rotation. Under 4°C thermal change, the free end has a pure 6.8 μm radial translation. By using inertial relief, the influence functions have been obtained and used to build a relationship between the transmitted loads and the mirror surface distortion. This relationship has been verified by comparing the result of superposing influence functions scaled by according transmitted load and with that of primary mirror assembly FEA model. According to the error budget and the influence functions, the permissible loads required of the flexure were directly established. The optimization was achieved through optimizing the compliance of the flexure under three simple load cases. With our method, the mirror design and flexure design has been decoupled, and time and resources required for optimization are reduced. The results after optimization have been within the error budget simultaneously.

Acknowledgments

The authors gratefully acknowledge support from the National Nature Science Foundation of China (NSFC) (Grant Nos. 11703027 and 61705223).

References

1. M. Kotani et al., "Quality evaluation of spaceborne SiC mirrors (I): analytical examination of the effects on mirror accuracy by variation in the

- thermal expansion property of the mirror surface," *Appl. Opt.* **52**(20), 4797–4805 (2013).
2. P. Bely, *The Design and Construction of Large Optical Telescopes*, Springer-Verlag, New York, pp. 1–28 (2003).
3. H. Kihm et al., "Adjustable bipod flexures for mounting mirrors in a space telescope," *Appl. Opt.* **51**, 7776–7783 (2012).
4. G. H. Xiong et al., "Deformation control by VSR technique on Al alloy thin-walled components," in *IOP Conf. Ser.: Mater. Sci. and Eng.*, Vol. 269, p. 012003, IOP Publishing (2017).
5. H. Kihm and H.-S. Yang, "Design optimization of a 1-m lightweight mirror for a space telescope," *Opt. Eng.* **52**(9), 091806 (2013).
6. Q. Xu and Y. Li, "Stiffness modeling for an orthogonal 3-PUU compliant parallel micromanipulator," in *Proc. 2006 IEEE Int. Conf. Mechatron. and Autom.*, IEEE (2006).
7. P. Zhou et al., "Research on neutral surface of lightweight, horizontally supported mirror," *Opt. Eng.* **57**(2), 025107 (2018).
8. L. Howell, *Compliant Mechanisms*, John Wiley & Sons, Inc., New York (2001).
9. S. Xiao, Y. Li, and X. Zhao, "Optimal design of a novel micro-gripper with completely parallel movement of gripping arms," in *2011 IEEE Conf. Rob. Autom. and Mechatron. (RAM)*, IEEE (2011).
10. S. Xiao, Y. Li, and Q. Yang, "A novel flexure-based 3-DOF micro-parallel manipulator with gripper for micro/nano manipulation," in *6th IFAC Symp. Mechatron. Syst. (Mechatronics)*, Hangzhou, IFAC, Vol. 46, pp. 606–611 (2013).
11. R. W. Besuner et al., "Selective reinforcement of a 2m-class lightweight mirror for horizontal beam optical testing," *Proc. SPIE* **7018**, 701816 (2008).
12. Y. C. Chen et al., "Study of bonding positions of isostatic mounts on a lightweight primary mirror," *Proc. SPIE* **8516**, 85160M (2012).
13. M. Laslandes et al., "Space active optics: performance of a deformable mirror for in-situ wave-front correction in space telescopes," *Proc. SPIE* **8442**, 844220 (2012).
14. H. An, D. E. Green, and J. Johrendt, "Multi-objective optimization and sensitivity analysis of tube hydroforming," *Int. J. Adv. Manuf. Technol.* **50**, 67–84 (2010).

Pingwei Zhou received his BS and MS degrees in mechanical engineering from Northwestern Polytechnical University in 2011 and 2014, respectively. He is currently working toward his PhD at Changchun Institute of Optics, Fine Mechanics and Physics, Chinese Academy of Sciences. His research interests include lightweight mirror design and space active optics.

Biographies of the other authors are not available.